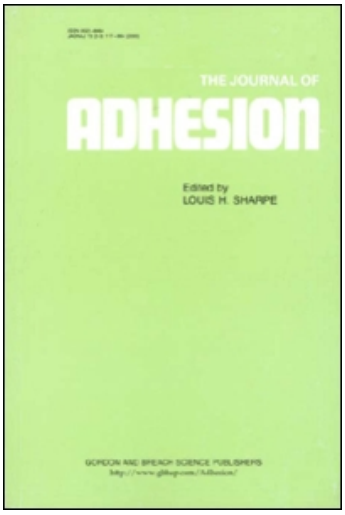

The Journal of Adhesion
Publication details, including instructions for authors and subscription information:
http://www.informaworld.com/smpp/title~content=t713453635

Penetration of Deposited Ag and Cu Overlayers Through Alkanethiol Self-Assembled Monolayers on Gold

G. C. Herdt[a]; D. R. Jung[ab]; A. W. Czanderna[a]
[a] National Renewable Energy Laboratory, Golden, CO, USA [b] SAIC, McLean, VA, USA

To cite this Article Herdt, G. C. , Jung, D. R. and Czanderna, A. W.(1997) 'Penetration of Deposited Ag and Cu Overlayers Through Alkanethiol Self-Assembled Monolayers on Gold', The Journal of Adhesion, 60: 1, 197 — 222
To link to this Article: DOI: 10.1080/00218469708014419
URL: http://dx.doi.org/10.1080/00218469708014419

J. Adhesion, 1997, Vol. 60, pp. 197–222
Reprints available directly from the publisher
Photocopying permitted by license only

Penetration of Deposited Ag and Cu Overlayers Through Alkanethiol Self-Assembled Monolayers on Gold*

G. C. HERDT**, D. R. JUNG*** and A. W. CZANDERNA†

National Renewable Energy Laboratory,
1617 Cole Boulevard, Golden, CO 80401, USA

(Received September 16, 1995; in final form March 28, 1996)

The purpose of our research is to study the reactions, interactions, or penetration between vacuum deposited metals (M) and the organic functional end groups (OFGs) of self-assembled monolayers (SAMs) on Au films under controlled conditions. Metal/SAM/Au systems are models for understanding bonding at M/organic interfaces and the concomitant adhesion between the different materials. In broad terms, the M/OFGs form interacting interfaces (*e.g.*, Cr/COOH or Cu/COOH) in which the deposit resides on top of the OFGs or weakly interacting interfaces through which the overlayer penetrates and resides at the SAM/gold interface. We present a review of XPS results from weakly interacting systems (Cu/CH_2OH, CU/CN, Ag/CH_3, Ag/COOH) and discuss in more depth the time-temperature dependence of the disappearance of the metal from the M/SAM interface following deposition using ISS on the Ag/CH_3 and Ag/COOH systems. XPS and ISS were used to characterize five alkanethiols terminated with CH_3,COOH(C–11 and C–16 chain lengths), CN and CH_2OH before and after depositing up to 1.0 nm Ag or Cu at *ca.* 10^{-7} torr. XPS spectra indicate that no strong interaction occurs between the deposited Ag and the COOH organic functional group, although a stronger interaction is evident on a C–16 COOH, and a unidentate is formed for Cu on the CH_2OH. An interaction between Cu and CN is evident, and penetration into the SAM occurs to a greater extent than for Cu on CH_2OH. The Ag interaction with CH_3 is weak. ISS compositional depth profiles for Ag on COOH and CH_3, taken from 113 to 293 K, indicate that Ag remains on the surface of the C–11 COOH for up to 1 h after deposition, whereas Ag penetrates CH_3 in less than 5 min at 295 K. The time for Ag to penetrate into a C–16 COOH is several times longer than for the C–11 COOH and depends on the SAM temperature.

KEY WORDS: Self-assembled monolayers (SAMs); polymer-metal interactions; polymer-metal interfaces; XPS/ISS analysis of polymer-metal interfaces; metal penetration through SAMs; metal penetration through polymers; Cu interactions with hydroxyl; Ag interactions with COOH; Ag and Cu deposited on CH_3; CN, CH_2OH, and COOH SAM end groups.

ABBREVIATIONS

BE	Binding Energy
CDP	Compositional Depth profiles

*Performed under DOE contract DE-AC36-83CH10093. Presented in part at the Eighteenth Annual Meeting of The Adhesion Society, Inc., Hilton Head Island, South Carolina, U.S.A., February 19–22, 1995.

**Performed as an Associated Western Universities Lab-Grad Fellow as part of his doctoral dissertation at the University of Denver.

***Present Address: SAIC, MS 231, 1710 Goodridge Dr., McLean, VA 22102, USA.

†Corresponding author.

FT-IRRAS	Fourier Transform Infrared Reflection Absorption Spectroscopy
ISS	Ion Scattering Spectroscopy
M or MO	Metal or Metal Oxide
M/SAM	Metal/Self-Assembled Monolayer
MDN	Mercaptododecanenitrile, $HS(CH_2)_{11}CN$
MHA	Mercaptohexadecanoic acid, $HS(CH_2)_{15}COOH$
MUA	Mercaptoundecanoic acid, $HS(CH_2)_{10}COOH$
MUO	Mercaptoundecanol, $HS(CH_2)_{11}OH$
NREL	National Renewable Energy Laboratory
ODT	Octadecanethiol, $HS(CH_2)_{17}CH_3$
OFG	Organic Functional Group
SAM	Self-Assembled Monolayer
XPS	X-ray Photoelectron Spectroscopy

1. INTRODUCTION

This review summarizes part of recent research[1-11] to elucidate penetration rates of metal overlayers through the SAM using ion scattering spectroscopy (ISS)[6,7] or to identify metal/organic functional group interactions at metal/self-assembled monolayer (SAM) interfaces, primarily by means of X-ray photoelectron spectroscopy (XPS).[1-5,8-11] As illustrated in Figure 1a, SAMs have fulfilled a need for model systems with ordered organic surfaces of uniform chemical composition for studying interactions at metal or metal oxide/organic interfaces.[1-11] In principle, atomically sharp interfaces can be formed between the deposited overlayer and the SAM surface. Chemical bonding at metal/organic interfaces plays an important role in the reliability and durability of many technological devices.[12] Bonding at metal/organic interfaces has been typically studied either by surface analysis of organic species adsorbed onto single crystal metal surfaces,[13,14] surface analysis of metallized polymers,[15,16] or by coating a metal oxide with a polymer. The chemical environment studied in the first type of experiment bears little resemblance to that present at polymer/metal (oxide) interfaces. In contrast, the lack of structural and chemical

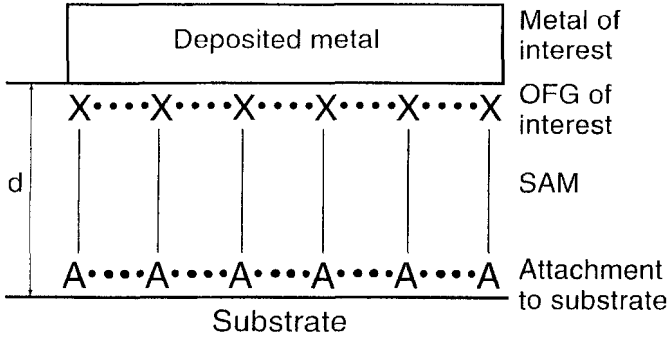

(1a)

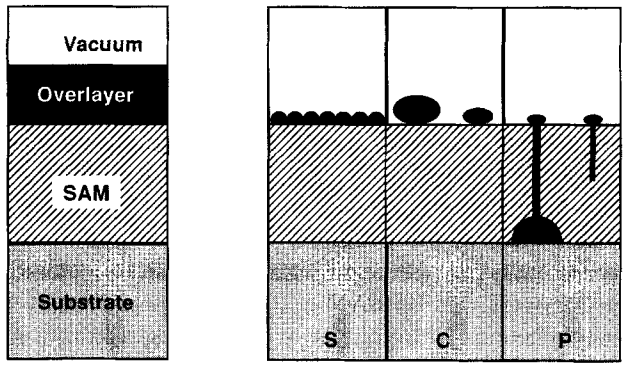

(1b)

FIGURE 1 (a) Idealized scheme for using an organized molecular assembly to form an interface between a metal overlayer and an organic functional group. The thickness of the SAM is d, and is the length of the molecule at perpendicular attachment. For alkane thiol SAMs on gold, the attachment group is a thiolate and the methylene chain is 28° from the normal at 295 K; (b) cross-sections of the principally observed results to date in which there is a (S) strong metal-OFG interaction, (C) weak metal-OFG interaction, or (P) very weak metal-OFG interaction. The designations S, C, and P stand for smooth, clustered, and penetrating, respectively.

order of polymer surfaces complicates the location and type of interactions with metal or oxide overlayers. MO or M/SAM studies have added a new approach in which the state of subdivision of the M or MO overlayer is different and selection of a highly ordered organic surface is possible.

Reactive transition metals (*e.g.*, Cr and Ti) are frequently used to promote adhesion at metal/polymer interfaces, and have been the subject of many studies.[5,11,17–20] Good metal adhesion on polymers with oxygen functionalities is well known and can be two to 10 times better than on polymers without oxygen-bearing groups.[15,16] Less reactive metals (*e.g.*, Ag and Cu) are frequently used as metallization coatings of polymers, for mirror applications, or as grid lines in photovoltaic cells, which may contain polymer/metal interfaces. For studying the stability or reactivity of interfaces, SAMs are ideal because they form ordered, thermally-stable arrays of close packed aliphatic chains terminated by a surface of uniform chemical functionality, as originally cited in the work of Allara and Nuzzo[21,22] and recently reviewed by others (Table I).[23] SAMs with a variety of terminating functional groups are now available, making studies of the interaction between an organic surface of a

TABLE I
Some Properties of Thiol/Au SAMs as Summarized by Dubois and Nuzzo[23]

Strength of Au thiolate bond	~44 kcal/mol
Superlattice of S head groups on Au(111)	$(\sqrt{3} \times \sqrt{3})$R30°
S-S nearest-neighbor spacing	0.449 nm
Tilt angle of methylene chain axis on Au(111) from surface normal	~25—30°
Twist angle of the C-C-C plane from the plane containing the chain axis and the surface normal	~52°
T at which significant chain disordering occurs	~380 K
T at which a C22* thiolate monolayer decomposes/desorbs	~500 K

*C22 indicates the number of C atoms in each thiol molecule

known functionality and a known metal species possible. SAMs can be formed from alkyl sulfides, alkane acids, alkane thiols, and other more complex molecules on different surfaces, *e.g.*, Ag, Au, SiO_2, Al_2O_3, and GaAs and present tilt angles ranging from 0° to between 50° and 57° to the substrate,[24] packing densities and contact angles with water or hexadecane. Progress in studying alkane thiol SAMs terminated with CH_3, CH_2OH, COOH, $COOCH_3$, and CN with Ti, Cr, Cu, Ni, Al, K, Na, Ag overlayers has been summarized and critically reviewed.[10] The specific M/OFG combinations studied to date are identified in Table II.

In support of the main goal of recent M/SAM research (understanding the interactions between M overlayers on SAMs), the *objectives* of recent work have been to: (a) identify new chemical compounds or complexes, and intermediate stages in compound formation, if any; (b) establish which or what combination of the three main configurations of metal that may be present as a function of the ratio of deposited metal atoms to SAM organic functional groups (OFGs), as illustrated in Figure 1b: S (smooth metal) that is chemically bonded or complexed with the SAM and probably spread out on top of the SAM, C (clustered) nonbonded metal that is on top of the SAM and probably in the form of large clusters, and P (penetrating) nonbonded metal that significantly penetrates the SAM and whose morphology could take many forms; (c) compare the quantities S, C, and P for deposition at different rates on surfaces at different temperatures, and thereby search for evidence of activated processes, metastable/nonequilibrium states, and results that depend on the degree of SAM ordering; (d) obtain images of clusters on the SAM (by scanning probe or electron microscopy), and use the distribution of cluster sizes, the rate of deposition, and the surface temperature as parameters to model the kinetics of cluster nucleation and growth; (e) characterize the degree of ordering and close packing of the SAM before and after metallization (are pinholes playing a role?); and (f) measure rates of penetration of metal through the SAM.

The lowest energy state of a M/SAM system is that for which all the deposited metal forms between the substrate and the SAM, because the surface free energies of metals are much higher than those of organics. Thus, two critical questions about M/SAM research are: are the configurations S and C of Figure 1b stable at room temperature, and what factors determine that stability? The scheme depicted in Figure 1b, and our corresponding identification of species S with chemical bonding

TABLE II
Matrix of Metal/Organic Functional Group Systems $Au/HS(CH_2)_n—X, (X=OFG)$ Studied to Date

Metal \ OFG	CH_3	CH_2OH	$COOCH_3$	COOH	CN
Ag	ref. 6ab			ref. 6c	
Cu	ref. 58	ref. 3	ref. 8, 27, 11c	ref. 1, 2, 22	ref. 4, 8
Ni				ref. 10	ref. 5
K			ref. 10		
Na	ref. 10				
Al	ref. 10		ref. 10		
Cr	ref. 11a		ref. 8, 11c	ref. 11b	refs. 5, 8, 11a
Ti	ref. 9	ref. 9	ref. 9	ref. 9	

and species C and P with nonbonding, are intended as idealizations (*e.g.*, we neglect the role of metal carbide formation which could occur along the entire chain).

Objectives (c) and (e) listed above are concerned with *how* a M/SAM system attains the observed chemical state and spatial distribution. The process of adlayer nucleation and growth, a competition that is kinetically dependent on surface temperature and deposition rate, may be considerably more complex than that found for two-dimensional systems if there is diffusion into (and not just over) the SAM. The mechanism of penetration may involve different possible rate limiting steps, for example, lateral diffusion leading to penetration at defect sites *vs.* direct vertical diffusion that might be enabled by thermal motion (because of ambient thermal energy or transient thermal energy imparted by atom impact), chemical reaction with and saturation of the OFG, or disordering due to strong chemical effects.

The order, structure, and stability of alkanethiols monolayers on Au have been reviewed by DuBois and Nuzzo[23] and are briefly summarized in Table I. As implied, SAMs spontaneously self assemble but are also robust and stable. The characteristics of the ordered SAM include: (1) the presence of the desired OFG at the vacuum/SAM interface; (2) a low density of pinholes in the film; (3) uniform film thickness; (4) uniform average orientation of constituent molecules; (5) a low population of gauche bonds in the methylene chains; (6) lateral ordering (real-space Bravais lattice or translational symmetry vectors) and internal structure of the unit cell of the SAM monolayer; and (7) a domain size of coherent lateral order. Details of experimental probes used to characterize the properties of SAMs have been critically reviewed.[10] For stability, SAMs withstand extended atmospheric exposure, repeated washing, and temperatures from 60°C to 100°C. These and other film characteristics (*e.g.*, their wettability by water and other liquids) are described further by Dubois and Nuzzo.[23] Only a few of the objectives (a)–(f) and control of the characteristics (1)–(7) are addressed in this summary of part of the work done to date.[10]

For prior studies *directly related* to the research in the *partial* review, we include the work by Tarlov[7] and by us[6] on the Ag/ODT and by us on the Ag/COOH interfaces for SAMs on Au films. Using ISS, Tarlov showed that Ag deposited onto ODT at 300 K penetrates to the ODT/Au interface, but that Ag resides at the methyl end group when deposited at 90 K.[7] As we present below, Herdt and Czanderna studied the time and temperature dependence of Ag penetration through ODT, MUA, and MHA using ISS and showed that Ag penetrates rapidly through ODT above about 200 K, but penetrates less rapidly through MUA and MHA.[6]

The formation of Ag islands on Langmuir-Blodgett (LB) films made from cadmium arachidate, a polymeric phthalocyanine, and an alkyl-substituted polyglutamate statistical copolymer has been studied by Reiter *et al.* using X-ray reflectometry.[25] Their work indicates that 5 nm of Ag deposited at about 0.1 nm/s onto LB films formed islands that penetrated into the film to a depth of 1–2 monolayers, The interaction between vacuum-deposited Ag and poly(ethylene terephthalate) (PET) surfaces was studied by Gerenser,[26] who found evidence of charge transfer between deposited Ag atoms and the carbonyl O of PET at low Ag coverages. He also found evidence of additional bonding between vacuum-deposited Ag and plasma-induced COOH groups after treatment with an O plasma. From his XPS results, he concluded that a unidentate Ag species is formed.

The interaction of Cu with the specific terminal OFGs on SAMs has been studied at NREL and elsewhere.[8,27] For a carboxylic acid end group, COOH, a unidentate copper complex is formed with the single-bonded oxygen atom.[1,2] The copper atoms of this complex exhibit a maximum charge of + 1 with one charged Cu per COOH group. For a hydroxyl end group, CH_2OH, a similar copper oxide species is formed.[3] The possibility of penetration of Cu deposits into or through CH_2OH and CN SAMs was addressed following the reported penetration of Ag through ODT by Tarlov.[7] We also summarize below the reported partial penetration of Cu through MUO that occurs for coverages greater than 0.5 nm.[3] Czanderna *et al.*[1,2] saw no evidence of penetration for Cu on the MUA.

Studies on the interaction of CN[28-30] and CO,[31] which is isoelectronic to CN^- on transition metal surfaces, have been made as model systems for elucidating the molecular orbital theory for bonding at surfaces. We summarize the inverse system, Cu atoms deposited onto a two-dimensional condensed phase of the organic ligand CN, which is a different approach.[4]

2. EXPERIMENTAL

A detailed list and critique of the experimental measurements used to characterize SAMs is available.[10] For the typical results presented in this article, the use of XPS and ISS will be described. The sample preparation methods described below are similar to those reported by other groups.

A. SAM Preparation

The SAMs were formed by immersing clean Au-coated Si⟨100⟩ wafers in ethanolic solutions of octadecanethiol (ODT, $HS(CH_2)_{17}CH_3$), 12-mercaptododecanenitrile (MDN, $HS(CH_2)_{11}CN$), mercaptoundecanol (MUO, $HS(CH_2)_{10}OH$), mercaptoundecanoic acid (MUA, $HS(CH_2)_{15}COOH$, using the well-known self assembly process for alkyl thiols.[21,24,32] Some of the gold coatings were prepared by evaporating 80 nm of Au directly onto Ar^+ ion bombardment-cleaned Si wafer coupons,[33] while others were prepared by evaporating a 9 nm Cr adhesion layer followed by a 200 nm Au layer onto solvent cleaned Si wafers. The hillock sizes of these two types of Au films have been measured by STM and AFM to be 30–50 nm wide and 10 nm high for the Ar^+ ion sputtered substrates and about 100 nm wide and 10 nm high for the Cr-adhered Au films. In most cases, the Au surfaces were placed in a UV-ozone cleaner for 5 min to remove trace organic contaminants[34] prior to immersion in the (typically) 2 mM ethanolic alkanethiol solutions. The ozone treatment for 1 h produces a 1.7- nm - thick Au_2O_3 oxide on the gold that is subsequently reduced during the SA process.[35] The SA was carried out in glass that was cleaned with piranha solution at 90°C and rinsed with absolute ethanol.[1,2] Water contact angles of less than 10° are observed on the Au surface only if such a cleaning procedure is used. Following incubation times of 2–4 days at 295 K, a sample was removed, rinsed in ethanol, dried with ultra-high purity nitrogen, and checked with a Rame-Hart goniometer for a water contact angle to verify the presence of the SAM. Contact

angles of 10° to 20° ± 2°, 64° ± 2°, and 112° ± 2° observed in this study for the COOH-, CH_2OH-, CN- and CH_3-terminated SAMs, respectively, are in good agreement with published results.[32]

B. Evaporative Deposition of the Metal

Evaporative deposition of the metal onto the SAMs and subsequent X-ray photoelectron spectroscopy (XPS) and ISS analysis were carried out using a Leybold-Heraeus LHS-10 surface analysis system. The LHS-10 is equipped with an analysis chamber and a sample preparation chamber through which a sample introduction rod can be translated without breaking vacuum. The sample preparation chamber is equipped with two vacuum feedthroughs that provide power to crucibles used for evaporative deposition. Deposition rates are measured with a quartz crystal oscillator using an IC 6000 deposition monitor. A negligible amount of sample heating occurs during deposition because the sample-to-source distance is approximately 38 cm. An X-ray source for XPS analysis, an ion gun for sputtering and for ISS, and a concentric hemispherical energy analyzer (CHA) are attached to the analysis chamber. The CHA is used to determine the energies of scattered ions in ISS. A complete description of this apparatus and its use for XPS and ISS have been presented previously.[36]

C. XPS and ISS Measurements

With the sample mounted onto a hot/cold transfer rod (initially at 22°C) and inserted into the LHS-10 chamber that is maintained at a base pressure of $2-5 \times 10^{-8}$ Pa, deposition of the Cu or Ag (Metron, 99.999%) took place in the attached preparation chamber that permits *in situ* transfer of the sample to and from the XPS (or ISS) analysis chamber at constant temperature. The sample was allowed to outgas at room temperature for 1 h prior to heating or exposure to X-rays. In our standard procedure, the sample was characterized by XPS at 295 K, heated or cooled as desired, recharacterized by XPS, exposed to the first incremental deposition of metal, and again characterized by XPS.[1-6] Repeated deposition/characterization cycles were performed in some cases, resulting in total coverages of up to 2 nm. Thus, the photoelectron escape depths permitted us to probe for M/OFG interface effects throughout the incremental deposition processes. Typically, a time period of 2 h was required for each cycle of XPS characterization involving a survey spectrum and narrow scan spectra. The 2-h exposure is less than that known to damage SAMs.[11b] In this paper, we refer to the amount of metal deposited as a uniform coverage, *e.g.*, 1.0 nm Ag or Cu, as though it is uniformly covering the surface of the SAM. We are aware that clustering may occur, but must provide a frame of reference. We address the attenuation of the photoelectron peak intensities in models used to estimate the degree of clustering or uniformity of the M overlayer. In all experiments, less than 3 min elapsed between the end of metal deposition and the beginning of the XPS or ISS analysis.

The photoelectron spectra were recorded using a non-monochromatic Mg $K\alpha$ X-ray source operated at 240 W. Narrow scans were taken using constant pass

energies of 200 eV for N 1s (for coverages below 0.2 nm) and 50 eV for C 1s, N 1s, O 1s, Au 4f, Cu 2p and Ag 3d. Survey scans were taken in the constant transmission mode with a retardation ratio of 3. For determining XPS peak areas and binding energies, the C1s narrow-scan line shapes were fit with a linear background and 85% Gaussian-15% Lorentzian (G/L) product functions of appropriate peak widths for each of the high resolution scans,[37] and a linear background using a nonlinear least squares package.[38] The BEs of all peaks are referenced to the Au $4f_{7/2}$ peak position at 84.0 eV to account for sample charging, which was found to be negligible.[39] The XPS data are used to evaluate the interface stoichiometry from adjusted peak intensities, the "chemical state" from BE shifts, and nonchemical BE shifts for partial to total penetration.

ISS compositional depth profiles were measured using 1 keV $^3He^+$ ions at a current density of 0.2 $\mu A/cm^2$ and temperatures from 113 to 295 K. The *ca.* 1-mm FWHM ion beam was rastered over a 2 mm × 2 mm area with the detected signal gated at a 70% aperture to minimize the signal from the etch-pit walls. During ISS analysis, He from the ion gun caused the chamber pressure to increase from a base pressure below 2×10^{-9} Torr to a carefully maintained pressure of 4×10^{-7} Torr. Each ISS spectrum was acquired from 800 eV to 1000 eV (E/E_0 of 0.8 to 1.0) over a period of approximately 40 s. Detection of C with $^3He^+$ is limited by the number of H atoms bonded to the C. Carbon in CH_3 or CH_2 is difficult to detect with ISS, but C or CH exposed to the ion beam are detectable. Consequently, we did not attempt to detect C in our compositional depth profiles. Sulfur from the thiol has been observed by ISS in previous work.[33] Accordingly, data were taken over an energy range E/E_0 of 0.80 to 1.0, to obtain depth profiles with good time resolution and good signal-to-noise.

3. RESULTS AND DISCUSSION

We present and discuss in this section a summary of the M/OFG combinations studied to date and rank them according to their degree of penetration into the SAM.[10] We then present and discuss typical XPS results for the partial penetration of the Cu/CH_2OH and Cu/CN systems and the interactions of the Cu/CH_2OH, Cu/CN, Ag/CH_3 and Ag/COOH systems, and the XPS and ISS results for the complete penetration of Ag/COOH and Ag/CH_3.

A. Ranking of M/OFG Combinations According to Penetration

In Table III based on the XPS and FT-IRRAS results, we have ranked the penetration of the M/SAM systems according to the results reported for the different OFGs and different chain lengths of the SAMs. A dependence of the degree of penetration on the temperature of the sample, that is, lower penetration for lower temperatures, has been found for the the systems of Cr/CN, Ni/CN, and Cu/CN[5] $T \approx 173$ K, Ag/CH_3[6-7] $T \geqslant 90$ K, and Ag/COOH.[6c] A dependence on the length of the alkane thiol molecule may also affect the XPS results shown in Table III, that is, shorter molecules show evidence for permitting greater penetration.

TABLE III
XPS Evidence for Penetration in M/SAM Systems (All Au/S-$(CH_2)_n$-OFG) at Room Temperature (RT) and at Lower Temperatures (LT)

			Metal Shift		C 1s attenuation		Penetration		
n	Metal	OFG	RT	LT	RT	LT	RT	LT	Ref.
15	Ti	COOH	HBE	?	?	?	Very low	?	9
15	Ti	$COOCH_3$	HBE	?	?	?	Very low	?	9
15	Ti	CH_2OH	HBE	?	?	?	Very low	?	9
15	Cr	$COOCH_3$	HBE	?	?	?	Very low	?	8
15	Ti, Cr	CH_3	HBE	?	?	?	Low	?	5, 8, 9
15	Cr	CN	HBE	?	?	?	Low	?	8
11	Cr	CN	HBE	HBE	Slightly	OK	Low	Low	5
15	Cu	$COOCH_3$	HBE	?	?	?	Low	?	8
10	Cu	COOH	Zero	?	?	?	Low	?	1, 2
10	Cu	CH_2OH	LBE	?	Low	?	Moderate	?	3
11	Ni	CN	Zero	HBE	Low	Slightly low	Moderate	Low	5
15	Cu	CN	HBE	?	?	?	Low	?	8
11	Cu	CN	LBE	HBE	Quite low	?	Moderate	Low	4, 5
17	Ag	CH_3	LBE	HBE	Zero	?	High	Low	6, 7
10	Ag	COOH	HBE	?	?	?	Moderate	Low	42
15	Ag	COOH	HBE	?	?	?	Low	Low	42

Notes: The metal shift refers to whether a core level has been measured at low coverages to exhibit a high binding energy or low binding energy shift, HBE or LBE, respectively, with respect to the bulk metal core level. "C 1s attenuation" refers to the attenuation of the C 1s level compared to that expected for a uniform metal overlayer. References to the sources of these XPS results are given. Question marks (?) indicate that the information has not been reported. The degree of penetration is based on the authors' interpretation of the available XPS results, in which "very high" means the overlayer essentially resides in the same plane of the OFG and "high" means the overlayer penetrates to the Au/SAM interface.

We conclude from these rankings that the degree of penetration increases with decreasing reactivity. In order for the adsorbed metal atom or cluster to penetrate, it first must encounter the OFG. Penetration is unlikely if there is a reaction. If there is *no* reaction, then penetration can proceed in some cases. Rates of penetration have only been measured in the cases of Ag[6,7] and Na[40,41] on CH_3-terminated SAMs and for Ag on COOH-SAMs.[42] The reactivity is highest for the oxygen-containing OFGs, (except for Ag/COOH) intermediate for the CN OFG, and lowest for the CH_3 OFG.[10] For the metals, Ti is the most reactive, followed by Cr, Al, K, Ni, Cu, Na, and Ag, although the data for Al, K, Ni, and Na are scant. The decreasing reactivity within the transition metal series, Ti, Ni, and Cu, and the low reactivity of the noble metals, Cu and Ag, is in the same order as the filling of the *d* orbitals. The relative reactivity of trivalent Al and the monovalent alkali metals (Na, K) is not so clear at this point because so few of these M/SAM systems have been explored. Evaporating oxygen-free Al films has not been successful, as yet.[43] The M/SAM studies involving Al evaporation may have been affected by rapid oxidation of the deposit,[43] which would have had a severe effect on the chemical interactions at the interface.

There is some evidence that the reactivity of the SAM with the incoming M is also dependent on the SAM temperature.[5,11] Activation of M/SAM reactions may be because of electronic, steric, or structural factors and is not unexpected. Further

temperature-dependent studies are warranted in order to learn more about activation energies in M/SAM reactions as well as for rates of penetration.

B. Weakly Interacting Systems: Ag/CH_3, Ag/COOH, Cu/CN, and Cu/CH_2OH

(i) *XPS of Cu/CN* Both peak positions and changes in their relative amplitude have been examined.[4] From the narrow scan results for C 1s, N 1s, and Cu 2p (Fig. 2), we concluded that a 0.6 eV BE shift in the N 1s resulted from a net transfer of electronic charge from Cu to nitrogen. A shift of 1.5 eV to HBE in the Cu 2p 3/2 and a corresponding shift of 0.61 eV to a lower binding energy for the C 1s peak from the C in CN were used to conclude that the Cu(CN) interaction is weak. A detailed table of

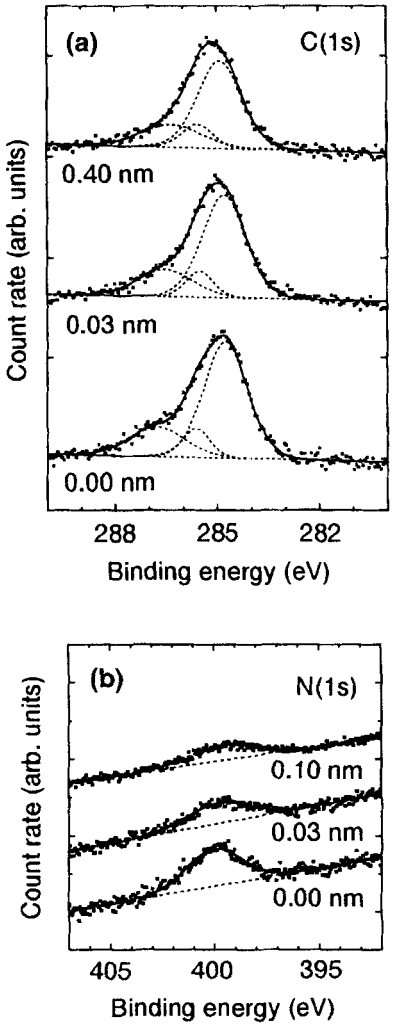

FIGURE 2

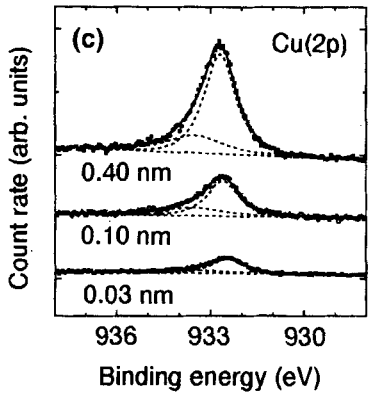

FIGURE 2 XPS narrow scan spectra (50° takeoff angle) at 295 K for the (a) C 1s, (b) N 1s, and (c) Cu 2p 3/2 lines for 0, 0.03, 0.1 and 0.4 nm Cu coverages.

position, width, and area from curve fitting these three peaks for Cu overlayer coverages from 0 to 6 nm is available.[4] Some of the BE shifts are evident in Figure 2. The peak intensities were analyzed in terms of possible models for the degree of penetration into the SAM, and the results are shown in Figure 3 for survey or narrow scan N 1s intensities as a function of Cu deposited.

The data in Figure 3 were normalized for comparison with model calculations that give the ratio of intensity, I, to the intensity that would be found for a bulk sample, I_B. The C, N, and Au data were normalized to the model intensities at 0 nm coverage. The Cu data were scaled to the model intensity at 10 nm coverage.

With the exception of the very lowest coverages, the observed decay in carbon intensity is much less than that predicted by an "ideal" model (M1 of Fig. 3) consisting of homogeneous, parallel layers in the sequence Cu/SAM/Au and incorporating the appropriate inelastic mean free path[44] and takeoff angle factors.[45] This lower attenuation rate can result from extensive penetration of the Cu into the SAM. The N attenuation rate, however, is in fair agreement with the model, except for the sharp drop between 0 and 0.03 nm coverage. In fact, a steep drop is also seen, but to a lesser degree, in the C data for the very lowest coverages. Either N is lost from the sample (perhaps, because of X-ray induced damage) or the N photoelectron flux is attenuated by the Cu overlayer. Rearrangement of the SAM structure could also be induced by the metal deposition. These possibilities may be accompanied by lateral and vertical distributions (*e.g.*, clustering) of the deposited Cu that are not easily modeled. Nevertheless, because the Au attenuation agrees well with the smooth overlayer model and the C attenuation is clearly very weak, we compare the date with a second model (M2 of Fig. 3) that considers the effect of penetration, without other possible factors. Because of the sharp initial drop in the C and N intensities, we have also included the effect of submerging the Cu/CN interface 0.35 nm below the original SAM/vacuum interface, but keep the total thickness of the SAM fixed at 17.8 nm. As seen in Figure 3, this assumption does not adequately account for the observed sharp drop in the N intensity. It does not affect the overall

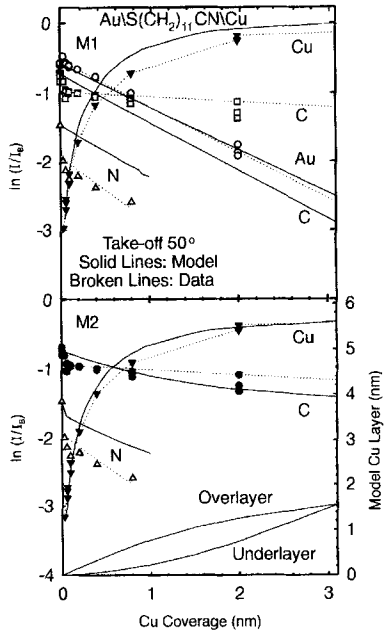

FIGURE 3 Survey spectra intensities at 295 K for Au, C, Cu, and N narrow scan intensities (takeoff angle 50°) *vs.* Cu thickness. The broken lines are linear fits to the data (symbols), except for the Cu broken lines that are merely guides to the eye. The solid lines are calculated assuming an ideal model (M1) in which all the Cu resides on top of the SAM and a model (M2) that includes penetration of the overlayer and a growing underlayer of Cu at the SAM/Au interface, *i.e.*, $(CH_2)_n/Cu/CN(CH_2)_mCu/Au$ interface, where the hydrocarbon layers n and m are 0.35 and 1.43 nm thick, respectively, and the two Cu layer thicknesses are indicated by the right ordinate.

slope of the N model curve, which is still determined by the inelastic mean free path for Cu, and by the amount of Cu located above the N layer.

Thus, in model M2, we assume that the Cu is distributed in two laterally homogeneous layers, one located at the Au/SAM interface and the other located just below the vacuum interface. The major modeling variable is the fraction of Cu that penetrates into the Au/SAM interface. In model M2, for the lowest coverages, a large fraction of Cu is located at the CN interface, but with increasing coverages, the Cu penetrates towards the Au interface. This model supports that penetration is a significant process in the Cu/CN system, but does not rule out or limit the other possible factors that would further explain our observations.

The possible contribution of X-ray damage to the measured N intensities was assessed in Ref. 11a. For the Cr/CN system with a 0.06 nm Cr deposit, the N 1s peak areas and BE shifts for samples exposed to X-rays prior to deposition were compared with those of a sample that was metallized prior to X-ray exposure. At 22°C, there was no significant difference, indicating that an approximately 1.5 h X-ray exposure prior to metallization did not greatly affect the experimental results. For sample temperatures of 50°C and 100°C, the N 1s peak area was much smaller in the case of X-ray exposure prior to deposition, and the BEs were shifted to a lower BE by 0.5 eV. In Ref. 11b on the Cr/COOH system, the time constant was 2 h for

decay of the O 1s intensity during exposure to our X-ray source. Thus, X-ray exposure may explain in part the sharp drop in the N intensity found in Figure 3.

For low coverages in M2, the overlayer and underlayer thicknesses show that the penetration by the deposited Cu is slight; but for higher coverages, the underlayer and overlayer thicknesses are similar. In comparison with the Cu on $HS(CH_2)_{10}OH$ system,[3] the carbon attenuation here is less steep, while the nitrogen attenuation is steeper than that for the oxygen of the Cu/CH_2OH system (see below). Modeling of the Cu/CH_2OH system by model M2 (in which the Cu overlayer and underlayer locations were the same as described here, but in which the overlayer and underlayer thicknesses were different), yielded a greater fraction of Cu in the overlayer compared with the present case. This, and the greater prominence of the Cu high binding energy (HBE) shoulder for Cu/CH_2OH compared with Cu/CN, supports the conclusion that the amount of copper reaching the SAM/Au interface increases with decreasing OFG reactivity (Table III).

The attenuation of the carbon and nitrogen intensities (Fig. 2) is rapid below 0.1 nm and gradual thereafter, as are rates of change of the C HBE and N peak positions *vs.* coverage.[4] These results are consistent with the first half-monolayer or so of Cu being located near, interacting with, and saturating the CN groups of the SAM (at a Cu/CN ratio of 2). We can expect that the low coverage Cu film consists of clusters, although we have only indirect evidence for this in the LBE shift of the main Cu peak and in the lower intensities for the Cu data compared with M1 in Figure 3. After about 0.1 nm coverage, an increasing fraction of each increment of the deposited Cu apparently penetrates the SAM and shows relatively little affinity for, or effect on, the previously formed species.

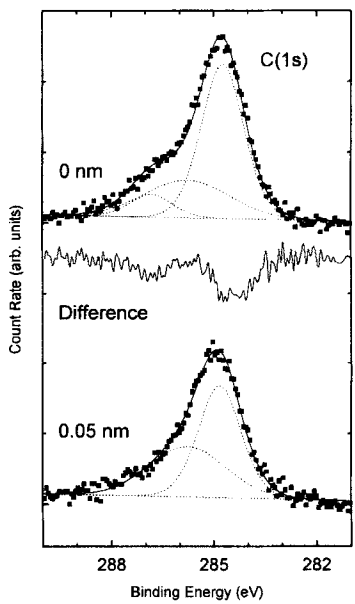

(4a)

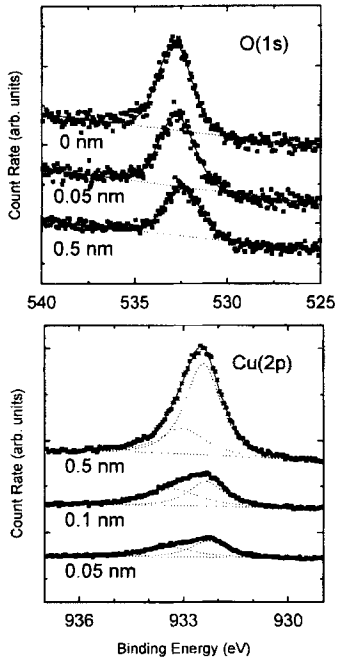

(4b)

FIGURE 4 (a) Carbon 1s XPS spectra at 295 K for 0 nm (upper) and 0.05 nm (lower) Cu coverage, and the difference spectrum (middle). (b) (Top) Oxygen 1s XPS spectra for 0, 0.05, and 0.5 nm Cu coverage; (Bottom) copper 2p XPS spectra for 0.05, 0.1, and 0.5 nm Cu coverage.

(ii) *XPS of* Cu/CH_2OH Peak positions and changes in their relative amplitude have been examined.[3] From the narrow scan results for C 1s, O 1s, and Cu 2p (Fig. 4), we concluded that a limited amount of Cu(I) oxide is formed with a shift of 1.1 eV to HBE at coverages below 0.5 nm, and is accompanied by a Cu(0) component that grows rapidly with increasing Cu coverage. The oxide is Cu(I) based on the Cu Auger emission and the Auger parameter calculated from the Auger kinetic energy and the Cu $2p_{3/2}$ BE at 932.3 eV. Changes in the C 1s and O 1s lineshapes are consistent with the low coverage interaction of Cu with the CH_2OH group. For example, the O 1s peak shifts very gradually to lower BE with no significant change in width until 3 nm of Cu coverage. This shift is consistent with increasing electron charge on oxygen, donated by Cu. A continuous shift of the oxygen peak, as tabulated in Ref. 3 for coverages above 0.1 nm, may result from the sharing of an increasing number of Cu atoms, *i.e.*, as the charge transferred per oxygen atom increases, the amount transferred per Cu atom decreases. The lack of a significant change in the oxygen line shape below 3 nm coverage supports the possibility that most of the oxygen experiences the same chemical environment and exhibits the same chemical shift.

Figure 5 shows plots of Cu 2p, O 1s, and Au 4f survey scan intensities (take-off 50°) at increasing Cu coverages that are normalized and compared with models M1 and M2, as was shown for Cu/CN. The penetration of Cu through the Cu/CH_2OH SAM is presumably prevented at low coverage by the reactive "cap-

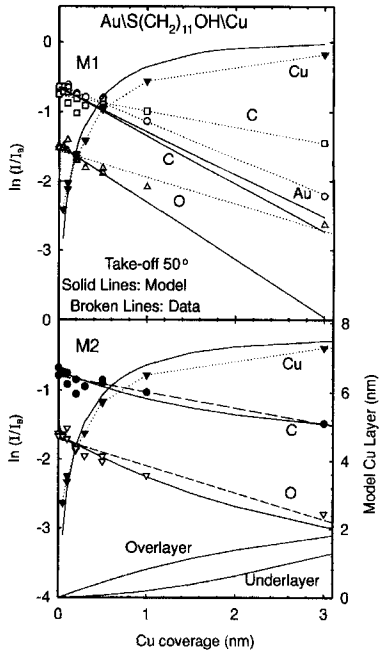

FIGURE 5 Survey spectra intensities at 295 Kv. Cu thicknesses at a 50° take-off angle, in which 90° is the surface normal. The broken lines are linear fits to the data, (except for the Cu broken lines that are merely guides to the eye). The solid lines are calculated assuming an "ideal" model (M1) in which all the Cu resides on top of the SAM and a model (M2) that includes penetration of the overlayer and a growing underlayer of Cu at the SAM/Au interface, *i.e.*, $(CH_2)_n/Cu/OH(CH_2)_mCu/Au$, in which the hydrocarbon layers n and m are 0.35 and 1.43 nm thick, respectively, and the two Cu layer thicknesses are indicated by the right ordinate.

ture" of the Cu by the CH_2OH functional group. No penetration was reported for Cu deposited onto a $COOH(CH_2)_{10}SH$/Au SAM.[1] In comparison with Cu/CN, carbon attenuation here is steeper, while the oxygen attenuation is less steep than that of nitrogen for the CN monolayer. In model M2 for Cu/CH_2OH, we find a greater fraction of Cu in the overlayer compared with Cu/CN. This and the greater prominence of the Cu HBE shoulder for Cu/CH_2OH compared with Cu/CN supports our generalization that the amount of copper reaching the SAM/Au interface increases with decreasing metal-organic functional group reactivity (Table III).

There is evidence in the C 1s spectra that at coverages below 0.1 nm the CH_2OH functional groups of the SAM take part in the Cu—O reaction. At higher coverages, further evidence for a Cu—O reaction could not be shown from our data. We conclude that a large fraction, if not all, of the CH_2OH groups have already interacted with Cu when 0.1 nm of Cu coverage is reached. A complete monolayer of Cu would be about 0.21 nm thick, assuming bulk (111) spacing, with a surface density of 17.72 atoms/nm^2. The density of thiol chains, assuming a $(\sqrt{3} \times \sqrt{3})$ R30° lattice on Au(111), is 4.6 nm^{-2}. At 0.05 nm copper thickness, we estimate that the ratio of Cu atoms to alkyl chains is already nearly one, which supports our conclusion about the amount of Cu—O reaction.

Some degree of Cu islanding or clustering is consistent with a high Cu/chain ratio upon saturation of the CH_2OH chain groups (and with the extent of disagreement between data and model for Cu and Au in Fig. 5), although we have not attempted to include this in model calculations. The HBE Cu peak increases until 0.5 nm coverage, which is another candidate for the saturation point, but it is not known whether the associated Cu species results entirely from SAM oxygen.

(iii) *XPS of Ag/COOH and Ag/CH_3* The Ag/MUA, Ag/MHA, and Ag/ODT systems were studied with XPS and ISS (section iv) at incremental Ag coverages. The

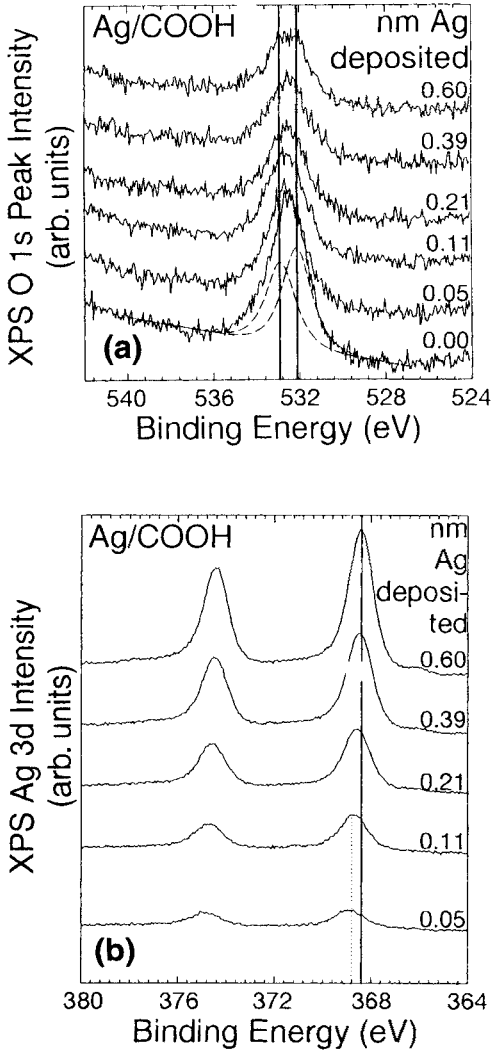

FIGURE 6

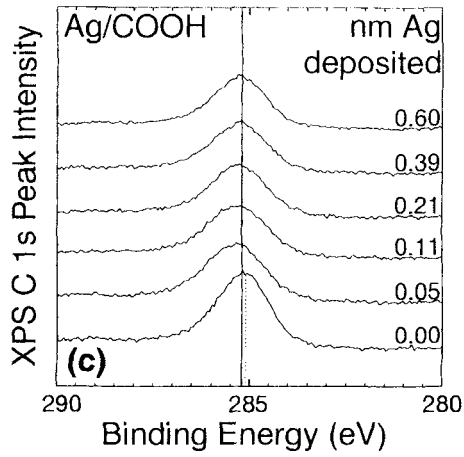

FIGURE 6 XPS line shapes for Ag coverages of 0.0, 0.05, 0.11, 0.21, 0.39, and 0.60 nm on COOH of MUA at 295 K for (a) O 1s, (b) C 1s, and (c) Ag 3d.

typical results reported here are for Ag/MUA for which we also have the most complete data. For the range of Ag coverages studied, results for the Ag/MHA and Ag/ODT systems are in good agreement with those for Ag/MUA, except O 1s data are not obtained from the Ag/ODT system. The O 1s XPS spectra of Ag on MUA as a function of Ag coverage are shown in Figure 6a. We determined from peak fits that these O 1s spectra could all be fit best with a low binding energy (LBE) peak at 531.9 eV and a high binding energy (HBE) peak at 532.9 eV and that the positions of the LBE and HBE components remain constant within experimental error for all Ag coverages studied for both Ag/MUA and Ag/MHA. Furthermore, the ratio of peak areas for the LBE and HBE peaks remains constant at 1:1 as a function of Ag coverage. These results do not indicate that a complex is formed between Ag and the COOH OFG, unless the interaction occurs without a detectable binding energy shift. If a complex were formed, we would have expected to observe the O 1s feature at 531.3 eV as previously observed in compounds with Ag bonded to O.[26,46]

XPS Ag 3d and C 1s spectra corresponding to the data in Figure 6a are shown in Figures 6b and 6c. With increasing Ag coverage, the Ag 3d peak position shifted to LBE by about 0.4 eV for Ag on MUA; for corresponding coverages, the Ag 3d shifted to HBE by about 0.1 eV for Ag on ODT.[6b] The XPS binding energy shift of the Ag $3d_{5/2}$ peak for Ag/ODT and Ag/MUA as a function of Ag coverage is shown in Figure 7. The binding energy shift differences probably result from initial or final state effects for Ag on metal (Ag/ODT, in which Ag resides at the ODT/Au interface) and Ag on an insulator (Ag/MUA).[47-50] The binding energy shift to HBE in the C 1s peak for Ag on MUA is about 0.2 eV(Fig. 6b), which is smaller than the value of about 0.4 eV for similar coverages of Ag on ODT.[6b] Coverage, temperature, and time-dependent factors could result in the observed XPS data, since final state screening of the core holds depends on the metallic properties and hence the cluster size. Other possible origins for the shifts in the C 1s peaks have been discussed by Tarlov.[7]

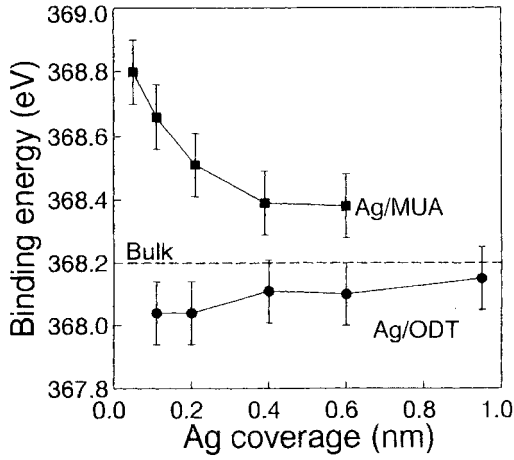

FIGURE 7 XPS Ag $3d_{5/2}$ peak binding energy shifts for Ag/ODT and Ag/MUA as a function of Ag coverage at 295 K.

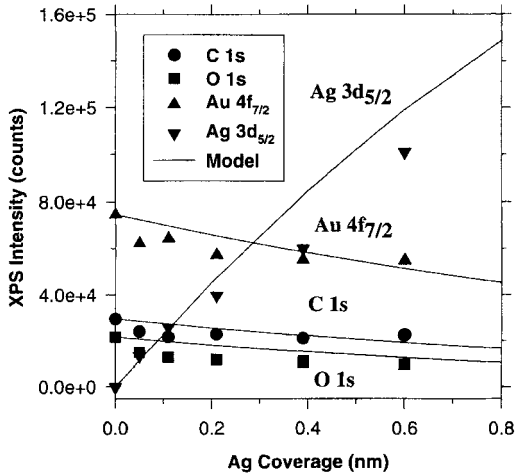

FIGURE 8 XPS intensities (areas) for Au $4f_{7/2}$, O 1s, C 1s, and Ag $3d_{5/2}$ for Ag coverages of 0.0, 0.05, 0.11, 0.21, 0.39, and 0.60 nm on MUA at 295 K.

Figure 8 shows the absolute XPS peak intensities as a function of Ag coverage on MUA. The solid lines in the figure correspond to intensities calculated assuming layer-by-layer growth of the Ag on the MUA. An unambiguous interpretation of these results is not possible. The intensities of the data are found to be less than that predicted by the model in all cases, which might be explained by X-ray damage to the SAM during the course of the experiments.[51,52] Similar behavior was observed for the Cu deposited onto CN for coverages below 0.6 nm, but above which the attenuation supported the hypothesis of overlayer clustering.[4] Fluctuation in the C 1s HBE data (corresponding to C=O bonded C) results from the relatively low

count rate measured for this peak. In contrast, Tarlov found no attenuation of the C 1s peak with Ag deposited to 1.0 nm at 295 K, which is consistent with rapid, complete penetration of Ag through the ODT he studied.[7]

(iv) *ISS CDP of Ag/CH_3 and Ag/COOH from 113 K to 293 K* ISS compositional depth profiles (CDP) were obtained from 113 to 293 K to study the penetration of Ag into ODT, MUA, and MHA, as a function of temperature. For all of these experiments, 1.0 nm Ag was deposited at a rate of approximately 0.01 nm/s onto the SAM prior to depth profiling. The elapsed time after starting metal deposition and completion of the first ISS spectrum was approximately 300 s (100 s, deposition; 160 s, sample transfer; and 40 s, first ISS spectrum). Thus, 5 min elapsed for time-dependent processes to proceed before our "initial" spectrum was taken during depth profiling. An ion beam current density of 0.2 μA/cm^2 was used for all ISS depth profiles. XPS and ISS measurements were carried out on several samples at 193 K and verified that no detectable oxygen signal could be obtained from the ODT samples. These data indicate that no ice formed on the samples during low temperature experiments.

The plots in Figure 9 show the *fraction* of Ag (Ag intensity divided by Ag intensity plus Au intensity) in the ISS depth profiles of Ag/ODT as a function of erosion time at temperatures from 113 to 293 K. The data are consistent with an increasing rate of Ag penetration to the ODT/Au interface at progressively higher temperatures, which results in greater Au intensities that are detected concomitantly with Ag when the Ag is at the ODT/Au interface. The time to erode through a "bare" ODT SAM to the ODT/Au interface[53] is about 1000 s at 0.2 μA/cm.[2] The plots in Figure 9 are consistent with a model of Ag residing on the methyl end group of ODT at liquid nitrogen temperatures and at the ODT/Au interface at 293 K.[6] The data also elucidate the temperature regime over which the rate of penetration increases rapidly. The residual Ag signal for erosion times greater than about 2000 s, which corre-

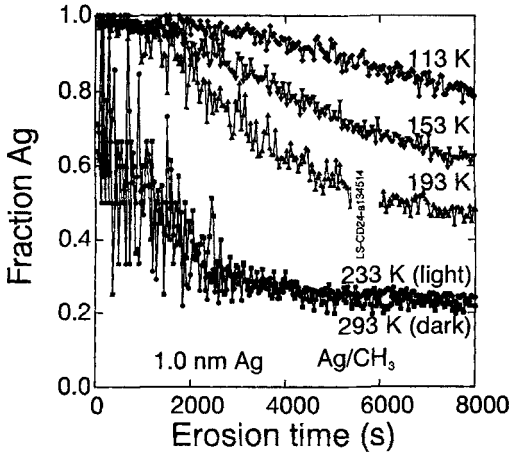

FIGURE 9 Fraction of Ag signal (see the text) as a function of erosion time at 0.2 μA/cm^2 for 1.0 nm Ag on ODT/Au at temperatures of 113, 153, 193, 233, 293K.

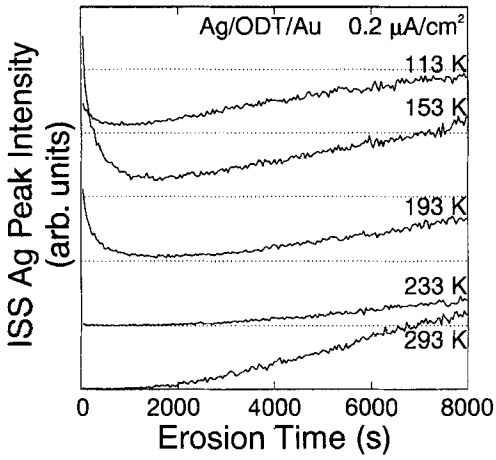

FIGURE 10 ISS Ag peak intensities as a function of erosion time at 0.2 μA/cm² for 1.0 nm Ag on ODT/Au at 113, 153, 193, 233, and 293 K. Each horizontal grid line represents the "zero" for the CDP above it. The distance between grid lines corresponds to equal integrated peak intensities. The initial spectrum for all ISS depth profiles is about 300 s after the onset of time-dependent processes (see the text).

sponds to the location of the ODT/Au interface, indicates the presence of Ag clusters at the ODT/Au interface.

Figure 10 shows the actual ISS Ag peak intensity (integrated peak area) as a function of erosion time for 113 to 293 K. Differences in the slopes of these CDPs for erosion times greater than 2000 s *may* reflect changes in the Ag cluster size or distribution at the ODT/Au interface (discussed more below), but other interpretations are possible given the complexity of this system. Since over three monolayers of Ag were initially deposited, substantial amounts of Ag must be in clusters at the ODT/Au interface because the Au signal is such a large fraction when the interface is reached, which is about 2000 s for eroding ODT when all the Ag penetrated to the ODT/Au interface. The amount of Ag that is in the SAM is likely temperature-dependent and difficult to quantify from the ISS experiments because of possible knock-in effects. The variation of the relative Ag and Au peak intensities as a function of temperature at erosion times of 2000 s indicate that 37% to 98% of the ODT/Au interface is covered by Ag.

The integrated initial ISS Ag peak intensities for Ag/ODT and Ag/MHA are shown as a function of temperature in Figure 11 and provides a measure of the maximum ISS Ag signal obtainable with our apparatus for 1.0 nm Ag before extensive penetration into the SAM has occurred. In contrast to Figure 9, the initial ISS Ag signal decreases above and below 153 K. The reproducibility of these data was carefully checked for coverages of 1.0 nm Ag. Two additional ISS compositional depth profiles were taken for a coverage of 5.0 nm Ag at 113 K to clarify the unexpected results below 153 K. The initial ISS signal intensity at 113 K and 5.0 nm Ag coverage is approximately the same magnitude as the data taken at 153 K with 1.0 nm Ag coverage. We have not determined if the Ag peak intensity is a maximum at 153 K (1.0 nm Ag) and 113 K (5.0 nm Ag).

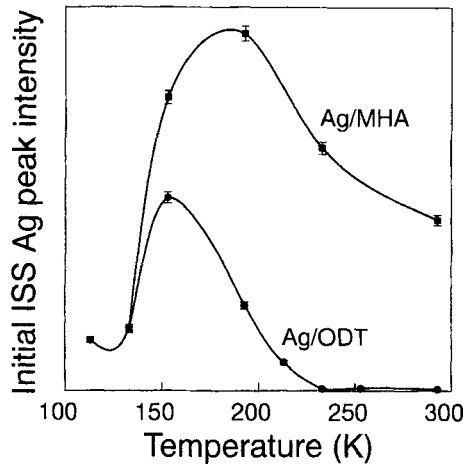

FIGURE 11 Initial ISS peak intensities for 1.0 nm Ag on MHA and ODT after deposition at temperatures from 113 K to 295 K.

Compared with ODT, the data for Ag/MUA (not shown) and Ag/MHA (Fig. 11) also show that a larger initial ISS signal is obtained. Data taken that are similar to those in Figure 9 show the rate of Ag penetration is slower for MUA than for ODT, and even slower for MHA. For example, the ISS peak area was measured at four different positions on the same sample for 1.0 nm of Ag on MUA and MHA as a function of time after deposition at 295 K after waiting for about 5, 15, 35, and 65 min after deposition; a fifth ISS Ag peak intensity was measured after 900 min for both MUA and MHA. As plotted in Figure 12, the data show that after deposition

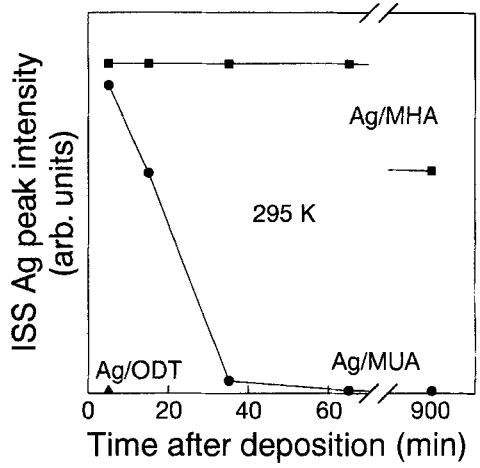

FIGURE 12 ISS peak intensities for 1.0 nm Ag on MUA and MHA as a function of time after Ag deposition at 295 K.

Ag remains on the surface of MUA for at least 5 min and some Ag is on the MUA surface for more than 1 h. For MHA, Ag remains on the surface for more than 1 h (*i.e.*, the Ag ISS intensity is unchanged), and the ISS intensity is only reduced to 68% of its initial value after 15 h, which shows that complete penetration to the SAM/Au interface is greatly retarded by the longer chain (C_{16} *vs.* C_{11}) MHA. By comparison, 1.0 nm of Ag penetrates ODT in less than 5 min at this temperature (Fig. 12). Ag on MUA is an intermediate case in which Ag remains on the surface for 5 to 15 min but then penetrates into the MUA, but 15% of the deposit is still on the surface after 1 h.

The slower Ag penetration through MUA and MHA compared with that for ODT at 295 K provides some indication of the mechanism of metal penetration through SAMs. First, weak interactions between Ag and the COOH group may retard the onset of Ag transport through MUA and MHA. We did not detect evidence for formation of a Ag unidentate complex with O, even though Ag—O interactions of 18 kcal/mol to 69 kcal/mol are known to exist.[54] Secondly, we speculate that at least partial hydrogen bonding between surface COOH groups, possibly having the "sideways dimeric" structure reported by Smith *et al.*,[27] restricts atom transport through the acid SAMs. However, the dimers do not necessarily result in an "ordered" surface network because their interactions disturb the potential for maximum packing density. *In situ* IR studies of the COOH surface are needed to clarify the type of hydrogen bonding in contrast to those[27] that permitted *ex situ* copper oxidation.[55] In addition to the likely absence of a Ag/CH_3 interaction, the CH_3 group on ODT experiences large rotational oscillations at 295 K[56] and so transport of Ag to the ODT/Au interface is not inhibited by OFG interactions. The increased rate of penetration of Ag through MUA relative to that for MHA is attributed to a greater movement of the OFGs in the less-tightly-packed, shorter-chain alkanethiol.[57] A third speculative possibility is that the presence of the COOH group on MUA and MHA reduces the number of defects in the SAM, so that fewer transport pathways are available in these films, again with the MHA more defect-free than for MUA.

In Figure 11, the initial ISS Ag peak intensities from CDPs of 1.0 nm Ag on MHA and ODT are compared for temperatures from 113 K to 295 K. The decrease in intensity below 150 K for ODT is challenging to interpret as transport to the interface. In the simplest case, the time-dependent processes relevant to understanding these results include nucleation and growth into clusters of deposited Ag, the cluster size distribution formed, and diffusion through the ODT or ODT domain boundaries to the ODT/Au interface. The latter depends on the integrity and reproducibility of the ODT SAM, *e.g.*, the number of pinhole defects in the SAM, gauche defects between chains above 200 K,[23] the nature of domain boundaries in the SAM, and other diffusion paths between the CH_3 end-group and the ODT interface. We *speculate* that the temperature for obtaining a maximum initial Ag signal depends on the amount and location of Ag deposited. For example, the rate of Ag lost from the clusters formed on the ODT surface is likely to increase at higher temperatures (diffusion) and decrease for larger clusters (less ODT defects available). The cluster size formed during the deposition typically decreases at lower temperatures and approaches a single or a few atoms. It is possible that such small "cluster" sizes at

113 K permits faster penetration than the larger cluster size formed at 153 K. At temperatures above 153 K, we suspect that the rate of diffusion through the ODT is the dominant transport mechanism. The cluster size at 5.0 nm Ag coverage at 113 K is expected to be larger than for 1.0 nm, and more Ag is initially present, which could explain why the Ag peak intensity is larger at 5.0 nm than at 1.0 nm of coverage. Obviously, changes in the mobility of Ag atoms at the surface and through the ODT as a function of temperature, and variations in the structure of the Ag/ODT/Au interfaces, play a role but are not known from our work.

As is seen in Figure 11, a similar decrease occurs for MHA, though below 200 K, and we think the reasons for the decrease are the same as presented above for Ag on ODT. The initial ISS Ag peak at 295 K for 1.0 nm Ag on MHA is more intense than the most intense initial ISS peak observed for 1.0 nm Ag on ODT. This result indicates that the Ag coverage of the COOH surface is higher, *i.e.*, the cluster size is smaller. Because the Ag initially remains longer on the COOH surface of MHA, the ISS signal can be a maximum for any given temperature, depending on lateral diffusion kinetics. Differences in Ag coverage on ODT and MHA probably result from differences in surface energy (and thus clustering) as well as on penetration of Ag through the two SAMs. In UHV, water desorbs, but the oxygen-containing OFG with some partial hydrogen bonding can (and probably does) play a role. SAMs are model systems for studying interactions at metal/organic interfaces. When metal penetration occurs, however, understanding the behavior of the model SAM systems being studied is complex. Factors dictating the specific structure of metal overlayers on SAMs might include metal nucleation behavior, SAM defect density and domain size, the chemical functionality of the SAM, and the available free volume between alkanethiol chains.

In summary, both the Ag/ODT and Ag/MHA systems show a marked decrease in ISS Ag signal intensity at temperatures below *ca.* 200 K, and the Ag ISS peak intensity for MHA remains consistently larger than that for ODT, even at lower temperatures. We interpret these results to mean that 1.0 nm Ag on MHA has more (and smaller) clusters that cover a greater surface area than 1.0 nm Ag on ODT, perhaps because of surface tension effects. We suggest that penetration of metal overlayers on SAMs may be linked to the available free volume between alkanethiol chains that constitute the SAM or at domain boundaries within the SAM. From this perspective, Ag penetrates MHA slowly at 295 K because partial hydrogen bonding between COOH OFGs inhibits motion of the alkanethiol chains, thus, limiting the access of surface Ag atoms into the free volume between the chains.[10] Furthermore, the ISS experiments show that the penetration processes are complex, and the models used for the XPS intensity plots do not adequately reflect the complexity. Further work is clearly needed to reveal the details of the Cr/OH or Cu/CN systems and should include using ISS.

Our research on the Ag/ODT and Ag/COOH systems shows that much work remains to be done before the behavior of weakly or noninteracting metal overlayers on model organic surfaces can be well understood. Using *in situ* AFM to understand the temperature-dependent clustering of Ag overlayers on SAMs and IR spectroscopy to probe changes in (weak) bonding at these interfaces should be especially valuable. Elucidation of metal nucleation and growth behavior on SAMs as a

function of temperature by use of AFM could play a key role in understanding the competition between the kinetics of metal cluster growth and metal diffusion through SAMs as a function of initial cluster size. The time evolution of the IR spectra of an Ag-metallized SAM could provide valuable information about specific penetration mechanisms. Detailed studies of Ag/SAM systems with selected OFGs may provide a basis for predicting the behavior of other metal/SAM systems with weak metal/OFG interactions.

C. Important Concerns about M/SAM Studies

Several important and crucial questions exist for M/SAM studies. These include: (a) are contaminants present in or on the film, (b) what kind of defects are in the SAM and at what density, (c) does the degree of penetration (Table III) increase with increasing SAM defect density, (d) does the SAM disorder significantly even for low metal overlayer coverages, and (e) what problems are caused by X-ray and e-beam exposures? None of the questions (a)–(e) seem unmanageable based on a recent review by Jung and Czanderna.[10]

4. CONCLUDING REMARKS

In the research to date, interactions of several M/SAM systems have been *identified*, along with *qualitative* relationships among the effects of chemical reactivity, temperature, and penetration of a metal/organic interface. With further research, the task remains to understand *quantitatively* how M/SAM interfaces are formed. This will require more complete characterization of the reactants, the structures, and the kinetics of the reactants and the structures of M/SAM systems.

The initial research on M/SAM systems, which was begun at NREL and initially reported in 1989 for Cu/COOH, Cu/CH_3, Cu/CN, and Cu/CH_2OH,[58] has served as a test of their use as model systems, and of whether M/SAM research will have benefits in applied areas, for example, real M/polymer interfaces. The results described above are clearly more readily interpreted and more detailed than most of their counterparts in the M/polymer interface literature. Based on the presence of similar reactants at a M/polymer interface, such as OFGs and metal atoms, this research approach succeeds in identifying factors that affect the initial bond between a metal and the polymer as the interface is formed in vacuum.

From the initial results, a continued broad effort is warranted for studying a matrix of 10 to 15 metals and metal oxides with about 10 different OFGs to evaluate the full potential of the approach and of this subfield of surface science. This should lead to the identification of submatrices targeted at specific classes of materials and applications.

Future characterization needs include obtaining (1) detailed, molecular orbital descriptions of new metal-organic bonds in a unique environment (because of the difference between bringing individual molecules to a metal surface compared with bringing individual metal atoms to an organic surface), (2) diffusion processes and rates for metals on organic surfaces, and (3) penetration processes and rates for metals into organic surfaces. These advances will be based on further work with

valence band probes, lateral imaging probes, and probes that can measure rates of penetration, as discussed above. Control of defects and a capability for the characterization of defects will be necessary to understand the relative role of intrinsic *vs.* extrinsic effects in chemical and physical processes in M/SAM systems.

Finally, the results of M/SAM studies may be applied to the understanding of M/polymer interfaces, and for this reason. M/SAM interfaces are often described as "model" M/polymer interfaces. Studies of metal oxides, semiconductors, and other inorganics deposited onto SAM substrates should provide results that can be applied to the understanding of other types of inorganic/organic interfaces. Further relevance to inorganic/organic interfaces actually used in practice and to interfacial reaction mechanisms under ambient conditions can be gained by exposure of inorganic/SAM interfaces to different atmospheres, temperature extremes, radiation, and chemical reagents. Inorganic/organic interfaces with well-defined and stable properties are needed in advanced devices.[59-61] Research to identify and modify reactions at inorganic/SAM interfaces will provide the fundamental understanding to fill that need.

Acknowledgments

The authors are pleased to acknowledge support by the U. S. Department of Energy under Contract DE-AC36-83CH10093 through the NREL's Director's Development Fund. We are especially grateful for the helpful discussions with D. L. Allara, P. Zhang, R. W. Collins, and D. E. King and to D. L. Allara and G. Whitesides for providing most of the alkane thiols we used in our experimental work. We thank D. L. Allara, P. Zhang, R. L. Opila, K. Konstadinidis, M. D. Porter, M. Grunze, H. G. Rubahn, L. H. Dubois, R. G. Nuzzo, M. J Tarlov, and P. Zhang for permission to use figures from their work in Ref. 10, and R. W. Collins, G. Scoles, A. J. Bard, J. E. Houston, K. H. Gray, R. W. Linton, S. M. Lindsay, G. N. Robinson, A. N. Parikh, K. Edinger, and F. Eisert for providing copies of their publications.

References

1. A. W. Czanderna, D. E. King and D. Spaulding, *J. Vac Sci. Technol.*, **A9**, 2607 (1991).
2. D. E. King, A. W. Czanderna and D. Spaulding, in *Metallized Plastics 3: Fundamental and Applied Aspects*, K. L. Mittal, Ed., (Plenum, NY, 1992), pp. 149–161.
3. D. R. Jung, D. E. King and A. W. Czanderna, *Appl. Surf. Sci.*, **70/71**, 127 (1993).
4. D. R. Jung, D. E. King and A. W. Czanderna, *J. Vac. Sci. Technol.*, **A 11**, 2382 (1993).
5. D. R. Jung and A. W. Czanderna, *Mater. Res. Soc. Symp. Proc.*, **304**, 131 (1993).
6. a. G. Herdt and A. W. Czanderna, *Surf. Sci. Lett.*, **297**, L109 (1993); b. *J. Vac. Sci. Technol.*, **A 12**, 2410 (1994); c. *J. Vac. Sci. Technol.*, **A 13**, 1275 (1995).
7. M. J. Tarlov, *Langmuir*, **8**, 80 (1992).
8. P. Zhang, Ph. D. thesis, Department of Materials Science and Engineering, Pennsylvania State University, 1993.
9. R. L. Opila, K. Konstadinidis, D. L. Allara and P. Zhang, *Surface Sci.*, **338**, 300 (1995).
10. D. R. Jung and A. W. Czanderna, *Crit. Rev. Solid State Mater. Sci.*, **19**, 1 (1994).
11. D. R. Jung and A. W. Czanderna, *J. Vac. Sci. Technol.*, (a) **A 12**, 2402 (1994); (b) **A 13**, 1337 (1995); (c) *Appl. Surface Sci.*, (1996) In press.
12. E. Sacher, J. J. Pireaux and S. P. Kowalczyk, in *Metallization of Polymers*, ACS Symposium Series, series editor, M. J. Comstock, (American Chemical Society, Washington, DC, 1990) and references therein.
13. F. P. Netzer and M. G. Ransey, *Crit. Rev. Solid State Mater. Sci.*, **17**, 397 (1992).
14. M. R. Albert and J. T. Yates, *The Surface Scientist's Guide to Organometallic Chemistry*, (American Chemical Society, Washington, DC, 1987).
15. J. M. Burkstrand, *J. Vac. Sci. Technol.*, **20**, 440 (1982).

16. J. M. Burkstrand, *J. Appl. Phys.*, **50**, 1152 (1979); **52**, 4795 (1981).
17. K. Konstadinidis, R. L. Opila, J. A. Taylor and A. C. Miller, in Ref. 5, 83–90.
18. S. G. Anderson, J. Leu, B. D. Silverman and P. S. Ho, *J. Vac. Sci. Technol.*, **A 11**, 368 (1993).
19. M. J. Goldberg, J. G. Clabes and C. A. Kovac, *J. Vac. Sci. Technol.*, **A 6**, 991 (1988).
20. J. L. Jordan, C. A. Kovac, J. F. Morar and R. A. Pollack, *Phys. Rev.*, **B 36**, 1369 (1987).
21. R. G. Nuzzo and D. L. Allara, *J. Am. Chem. Soc.*, **105**, 4481 (1983).
22. D. L. Allara and R. G. Nuzzo, *Langmuir*, **1**, 45 (1985); 52 (1985).
23. A. Ulman, *An Introduction to Ultrathin Organic Films*, (Academic, New York, 1991); L. H. Dubois, and R. G. Nuzzo, *Ann. Rev. Phys. Chem.*, **43**, 437 (1992).
24. D. L. Allara, *Crit. Rev. Surf. Chem.*, **2**, 199 (1993).
25. G. Reiter, C. Bubeck and M. Stamm, *Langmuir*, **8**, 1808 (1992).
26. L. J. Gerenser, *J. Vac. Sci. Technol.*, A **6**, 5 (1988).
27. E. L. Smith, C. A. Alves, J. W. Anderegg, M. D. Porter and L. M. Siperko, *Langmuir*, **8**, 2707 (1992).
28. J. A. Rodriguez and C. T. Campbell, *Surf. Sci.*, **185**, 299 (1987).
29. Z. Ru-Hong and C. Pei-Lin, *Surf. Sci. Lett.*, **243**, L49 (1991).
30. J. Billman and A. Otto, *Surf. Sci.*, **138**, 1 (1984).
31. H.-J. Freund and E. W. Plummer, *Phys. Rev. B*, **23**, 4859 (1981), and references therein.
32. C. D. Bain, E. B. Troughton, Y.-T. Tao, J. Evall, G. M. Whitesides and R. G. Nuzzo, *J. Am. Chem. Soc.*, **111**, 321 (1989).
33. D. E. King and A. W. Czanderna, *Surf. Sci. Lett.*, **235**, L329 (1990).
34. J. R. Vig, *J. Vac. Sci. Technol.*, **A 3**, 1027 (1985).
35. D. E. King, *J. Vac. Sci. Technol.*, **A 13**, 1247 (1995).
36. J. R. Pitts, Ph. D. dissertation, Department of Physics, University of Denver, CO, 1985.
37. P. M. A. Sherwood, in Practical Surface Analysis, Volume 1, 2nd ed., D. Briggs and M. P. Seah, Eds. (J. W. Wiley and Sons, Inc., New York, NY, 1990).
38. Using Peakfit (R) from Jandel software.
39. D. E. King, A. W. Czanderna and D. Spaulding, *J. Vac. Sci. Technol.*, **A 11**, 180 (1993).
40. K. Bammel, J. Ellis and H.-G. Rubahn, *Chem. Phys. Lett.*, **201**, 101 (1993).
41. F. Balzer, K. Bammel and H.-G. Rubahn, *J. Chem. Phys.*, **98**, 7625 (1993).
42. G. Herdt and A. W. Czanderna, *J. Vac. Sci. Technol.*, **A 13**, 1275 (1995).
43. Independent observations by D. L. Allara, *et al.*, at Penn State U. R. L. Opila, *et al.*, at ATT Bell Labs, and A. W. Czanderna, *et al.*, at NREL.
44. S. Tanuma, C. J. Powell and D. R. Penn, *Surf. Interface Anal.*, **17**, 911 (1991); P. E. Laibinis, C. D. Bain, and G. M. Whitesides, *J. Phys. Chem.*, **95**, 7017 (1991).
45. D. Briggs and M. P. Seah, *Practical Surface Analysis*, (Wiley, Chichester, 1983).
46. P. J. Trotter, M. G. Mason and L. J. Gerenser, *J. Phys. Chem.*, **81**, 1325 (1977).
47. G. K. Wertheim, *Z. Phys.*, **B 66**, 53 (1987); **D12**, 319 (1989).
48. G. K. Wertheim, S. B. DiCenzo, D. N. E. Buchanan and P. A. Bennett, *Solid State Comm.*, **53**, 377 (1985) and references therein. The sign of the surface core level shift resulting from band narrowing is not easily predicted for Cr because the 3d band is half filled.
49. S. B. DiCenzo and G. K. Wertheim, *J. Elect. Spect. Rel. Phenom.*, **43**, c7, (1987).
50. I. Jirka, *Surf. Sci.*, **232**, 307 (1990).
51. P. E. Laibinis, R. L. Graham, H. A. Biebuyck and G. M. Whitesides, *Science*, **254**, 981 (1991).
52. D. R. Baer, M. H. Engelhard, D. W. Schulte, D. E. Guenther, Li-Qiong Wang and P. C. Rieke, *J. Vac. Sci. Technol.*, **A 12**, 2478 (1994).
53. D. E. King and A. W. Czanderna, to be published.
54. A. W. Czanderna, *J. Vac. Sci. Technol.*, **16**, 408 (1977).
55. D. E. King and A. W. Czanderna, *Langmuir*, **10**, 1630 (1994).
56. A. Ulman, *Adv. Mater.*, **3**, 298 (1991).
57. M. Grunze, private communication to AWC.
58. D. Spaulding, M. S. thesis, Materials Science Dept., University of Denver, Denver, CO, 1989.
59. A. W. Czanderna and R. J. Gottschall, Eds., *Mat. Sci. Engr.*, **53**, 1–168 (1982).
60. J. D. Swalen, D. L. Allara, J. D. Andrade, E. A. Chandross, S. Garoff, J. Israelachvili, T. J. McCarthy, R. Murray, R. F. Pease, J. F. Robolt, K. J. Wynne and H. Yu, *Langmuir*, **3**, 932 (1987).
61. A. W. Czanderna and A. R. Landgrebe, Eds., "Current Status, Research Needs and Opportunities in Applications of Surface Processing to Transportation and Utilities Technologies", *Crit. Rev. Surf. Chem.*, **2** (Nos. 1–4) and **3** (No. 1), 1993.